Applied Radiation and Isotopes 221 (2025) 111797

Contents lists available at ScienceDirect

Applied Radiation and Isotopes

journal homepage: www.elsevier.com/locate/apradiso

RAPTOR-AI: An open-source AI powered radiation protection toolkit for radioisotopes

Hiroshi Watabe [a], Peter K.N. Yu [b], Dragana Krstic [c], Dragoslav Nikezic [c], Kyeong Min Kim [d], Taiga Yamaya [e], Naoki Kawachi [f], Hiroki Tanaka [g], Zoran Jovanovic [h], A.K.F. Haque [i], M. Rafiqul Islam [j], Gary Tse [k], Quinncy Lee [l,m], Mehrdad Shahmohammadi Beni [a,b,k,*]

[a] *Division of Radiation Protection and Nuclear Safety Research Center for Accelerator and Radioisotope Science, Tohoku University, 6-3 Aoba, Aramaki, Aoba, Sendai, 980-8578 Miyagi, Japan*
[b] *Department of Physics, City University of Hong Kong, Tat Chee Avenue, Kowloon Tong, Hong Kong, China*
[c] *Faculty of Science, University of Kragujevac, R. Domanovica 12, 34000, Kragujevac, Serbia*
[d] *Korea Institute of Radiological & Medical Sciences, 75, Nowon-ro, Nowon-gu, Seoul, Republic of Korea*
[e] *National Institutes for Quantum Science and Technology, Anagawa 4-9-1, Inage-ku, Chiba-shi, Chiba 263-8555, Japan*
[f] *National Institutes for Quantum Science and Technology, 1233 Watanuki, Takasaki, Gunma 370 1292, Japan*
[g] *Institute for Integrated Radiation and Nuclear Science, Kyoto University, 2-1010 Asashiro-Nishi, Kumatori-cho, Sennan-gun, Osaka 590-0494, Japan*
[h] *State University of Novi Pazar Department of Natural Science and Mathematics, Vuka Karadzica 9, 36300, Novi Pazar, Serbia*
[i] *Atomic and Molecular Physics Laboratory, Department of Physics, University of Rajshahi, Rajshahi 6205, Bangladesh*
[j] *Institute of Nuclear Medical Physics, AERE, Bangladesh Atomic Energy Commission, Dhaka, 1349, Bangladesh*
[k] *School of Nursing and Health Studies, Hong Kong Metropolitan University, Homantin, Kowloon, Hong Kong, China*
[l] *The Institute of Applied Health Sciences, The School of Medicine, Medical Sciences, and Nutrition, University of Aberdeen, Aberdeen, United Kingdom*
[m] *Faculty of Infectious and Tropical Diseases, London School of Hygiene and Tropical Medicine, London, United Kingdom*

ARTICLE INFO

Dataset link: https://figshare.com/articles/software/RAPTOR-AI_--_Radiation_Protection_Toolkit_for_Radioisotopes_with_Artificial_Intelligence/26751967, https://raptorai.io/

Keywords:
Radiation protection
Monte Carlo method
Open-source
Artificial intelligence
Nuclear radiation

ABSTRACT

Artificial intelligence (AI) has gained significant attention in various scientific fields due to its ability to process large datasets. In nuclear radiation physics, while AI presents exciting opportunities, it cannot replace physics-based models essential for explaining radiation interactions with matter. To combine the strengths of both, we have developed and open-sourced the Radiation Protection Toolkit for Radioisotopes with Artificial Intelligence (RAPTOR-AI). This toolkit integrates AI with the Particle and Heavy Ion Transport code System (PHITS) Monte Carlo package, enabling rapid radiation protection analysis for radioisotopes and structural shielding. RAPTOR-AI is particularly valuable for emergency scenarios, allowing quick dose dispersion assessments when a facility's structural map is available, enhancing safety and response efficiency.

1. Introduction

The Monte Carlo (MC) method found to be very useful in field of medical, radiological and computational physics, thanks to the exponential growth in computational resources (Le et al., 2017; Su et al., 2014; Acebrón and Ribeiro, 2016). Number of well-established MC packages were developed over the years such as; Monte Carlo N-Particle (MCNP) https://mcnp.lanl.gov/ (Goorley et al., 2012; Goorley et al.), Geant4 https://geant4.web.cern.ch/ (Agostinelli et al., 2003), FLUKA http://www.fluka.org/fluka.php (Böhlen et al., 2014; Ferrari et al., 2005), Particle and Heavy Ion Transport code System (PHITS) https://phits.jaea.go.jp/ (Sato et al., 2018; Iwase et al., 2002) and etc. These packages have the ability to model transport and interaction of primary and secondary ionizing radiation in complex 3-dimensional domains (Yu et al., 2023; Watabe et al., 2023; Shahmohammadi Beni et al., 2017, 2021). Considering these MC packages, users must prepare code scripts to model specific irradiation scenarios. An important application of MC methods is in radiation protection, in which the absorbed dose from ionizing radiation emitted from a specific radioisotope should be determined (Hsiao and Stewart, 2007; Koyuncu and Reyhancan, 2020). Furthermore, the effectiveness of shielding materials can be studied against a particular type of ionizing radiation emitted

* Corresponding author at: Division of Radiation Protection and Nuclear Safety Research Center for Accelerator and Radioisotope Science, Tohoku University, 6-3 Aoba, Aramaki, Aoba, Sendai, 980-8578 Miyagi, Japan.
E-mail address: ben.sh@tohoku.ac.jp (M.S. Beni).

https://doi.org/10.1016/j.apradiso.2025.111797
Received 10 November 2024; Received in revised form 3 March 2025; Accepted 18 March 2025
Available online 28 March 2025

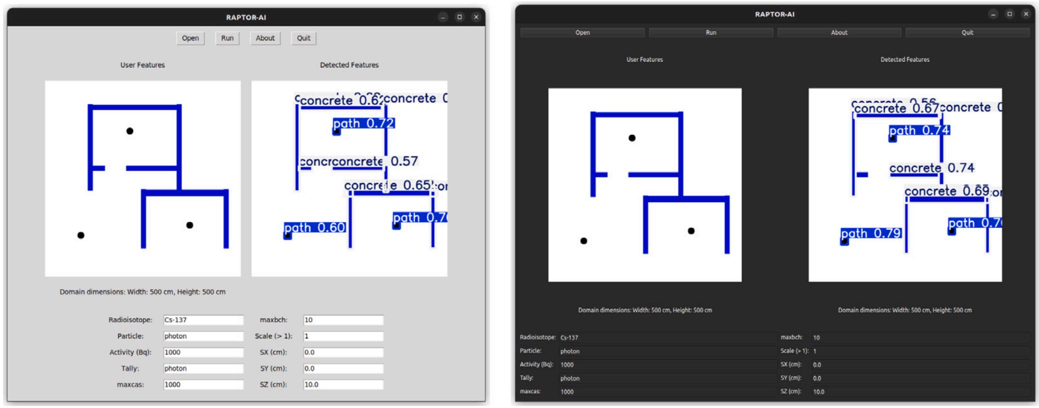

(a)   (b)

Fig. 1. RAPTOR-AI GUI (a) Tkinter and (b) Qt version in action using two different trained models to detect features on uploaded user image.

from a radioisotope (Aygün, 2021; Singh et al., 2013; Shahmohammadi Beni et al., 2021); this is mainly important in reducing the absorbed dose in organs and in turn minimizing the detrimental effect of ionizing radiations emitted from radioisotopes to living organisms.

In recent years, artificial intelligence (AI) has gained significant popularity in variety of scientific and engineering fields and applications; this is mainly due to the advancements in computational resources and abundance of data for training these AI models. The employment of object detection (Zhao et al., 2019; Zou et al., 2023) and natural language processing (Khurana et al., 2023) AI models found to be promising in variety of field such as; medical, finance, face recognition and education. Previously, the use of convolutional neural network (CNN) was used in the development of MCDNet (Monte Carlo Denoising Net) (Peng et al., 2019), with the ultimate goal of achieving acceleration in the MC dose calculations in radiotherapy; this denoising network was found to be promising in predicting high photon dose maps from low photon dose with 10x speed-up in terms of photon numbers used in the MC computations. Furthermore, Kimura and Nadege (2020) developed a region of interest (ROI) editing tool using NVIDIA Clara that has the ability to extract tumor or organs regions using AI from DICOM medical images. In recent years, artificial intelligence (AI) has become a powerful tool for automated recognition and analysis of ion tracks in solid state nuclear track detectors. By leveraging deep-learning algorithms, researchers have demonstrated significantly improved detection accuracy and efficiency compared to traditional image-processing methods. For instance, an AI-based track identification framework presented by Kuramitsu et al. (2024) employs convolutional neural networks to precisely classify and quantify tracks, underscoring the potential of machine learning approaches to streamline data processing and enhance the reliability of radiation measurements. Sarrut et al. (2021) reviewed the recent usage of AI method for MC modelings with the main focus on dose estimation with convolutional neural networks, dose denoising from low statistics MC simulations, detector modeling and event selection with neural networks. They have noted that the modeling heavily relies on the employment of large amount of datasets to perform training heuristically. In addition, the MC models that will be used to generate training data need to be prepared precisely and skillfully, and in conclusion they have concluded that "*For the moment, even if it is envisioned that deep learning can improve simulations, it does not seem certain that it can always replace Monte Carlo.*" (Sarrut et al., 2021).

Considering the fact that MC computations are an essential component of radiation physics studies and are also necessary for creating training datasets for AI models, it is pertinent to develop AI powered tools in conjunction with well-established MC packages, leveraging their accuracy, robustness and functionalities while improving usability and minimizing errors, rather than aiming to replace it with the AI. Considering this case, we have developed the Radiation Protection Toolkit for Radioisotopes with Artificial Intelligence named RAPTOR-AI using deep learning objection detection model. In this model, human phantom movement and multiple slab shielding materials can be generated with simple 2-dimensional markup images. In addition, custom-made code editor and image viewer was developed and bundled with the present program (see the supplementary material for further details). The present toolkit and obtained results would be useful in radiation protection studies, providing the users with a swift and precise method to perform radiation protection studies in scenarios that require immediate attention or in teaching and training.

2. Materials and methods

2.1. Program structure

Two different versions of the present program was developed, namely, (1) Tkinter, and (2) Qt applications. The Tkinter version of the present model, utilizes the python Tk GUI libraries to create the GUI for interaction of users with the program. On the other hand, the Qt version of the present mode utilizes the PyQt comprehensive set of Python bindings for Qt version 6.

The present program has two main parts that are the (1) AI object detection and (2) anthropomorphic human phantom generator module. The initial part of the program is responsible to load the GUI module, read user inputted configurations, process the user uploaded image, run the object detection AI using our trained model and present the processed image with detected features. The widely used YOLO (You Only Look Once) (Redmon et al., 2016) state-of-the-art, real-time object detection system version 5 which is based on Yolov1-Yolov4 (Xu et al., 2021) was used to train an AI model to detect these features. The detected features that were obtained from this module including the user inputted parameters would be passed to the anthropomorphic human phantom generator module. Firstly, the user-defined parameters such as the type of radioisotope, incident particle, source activity, tally type, source position in 3-dimensional coordinate system, number of histories and batch runs would be used to setup the MC model. In addition, the user set data for shielding materials and PHITS run parameters would be read from a *config.ini* file that is designed to allow the users to initialize their modeling configuration. The trained model and the confidence cutoff can be also set by the user using *model_loader.ini* file.

Algorithm 1 The Developed RAPTOR-AI Inference Process Algorithm

```
Load Configuration: Load modelname and modelconfidence from model_loader.ini
Initialize GUI components (Frames, Labels, Buttons, Entries)
Initialize user-controlled parameters: radioisotope, particle, activity, tally, maxcas, maxbch, scale, sx, sy, sz
Load Image: UploadImage
if Image is loaded then
    Display Image Dimensions as Width and Height
end if
Run Inference: RunInference
Set Paths: yolov5_path, weights_path, source_dir, output_dir
Execute YOLOv5: RunSubprocess
Save Coordinates: Save bounding box coordinates for detected objects
for each row in csv file do
    if prediction is shield then
        Save Shield Coordinates
    else
        Compute Center of Bounding Box
        Append Center Coordinates
    end if
end for
Sort and Save Center Coordinates
Generate Phantom: PhantomGeneration(countx, center_x, flipped_center_y, radioisotope, ...)
Display Inferred Image: Display the processed image with detections
```

The anthropomorphic human phantom generator (PhantomGeneration) module uses all the user-defined data and those features that were detected by the our trained AI model such as human phantom location and shielding size and locations to create a PHITS executable model of the modeled setup. The source type is fixed to point source with user-defined radioisotopes resembling common radioactive sources that emit incident particle in isotropic fashion which is defined using PHITS *s-type = 9* and *e-type = 28* functionality. The isotropic radioisotope point source location will be automatically set using user-defined *sx*, *sy* and *sz* from the GUI that corresponds to x, y and z position of the source, respectively. In the current version of the RAPTOR-AI we only support radioisotope point sources, however, ionizing radiation can emerge from other sources such as particle accelerators (Watabe et al., 2024a) and galactic cosmic rays (Badhwar, 1997). The core functionality and the inference process of the RAPTOR-AI is summarized in Algorithm 1. In addition, a brief overview of the functionality of the anthropomorphic human phantom and model generation using the detect features and user-defined inputs is shown in Algorithm 2 and Algorithm 3.

All the source codes can be downloaded freely from: https://figshare.com/articles/software/RAPTOR-AI_--_Radiation_Protection_Toolkit_for_Radioisotopes_with_Artificial_Intelligence/26751967. We refer the interested readers to the official website of the RAPTOR-AI (https://raptorai.io/) to access the online step-by-step user manual and to download the latest trained models. We will actively enhance our trained models that will provide new features and high precision in detecting features from 2D markup images. RAPTOR-AI is coupled with and uses the widely used PHITS Monte Carlo package, which has already been validated against accelerator-based measurements (Sihver et al., 2007). In addition, previous comparisons of PHITS and MCNP for neutron shielding in HDPE materials have shown good agreement with experimental data (Unagar et al., 2024).

Algorithm 2 The Developed Phantom and Model Generator Module Algorithm

```
function READ_COORDINATES_FROM_FILE(file_path)
    Input: Path to the file containing shield coordinates
    Output: List of coordinate dictionaries
    Open file at file_path
    Skip header line
    while lines remain in file do
        Split line by commas and convert to float
        Append dictionary of coordinates to list
    end while
    Return coordinates list
end function
function CHECK_OVERLAP(box1, box2)
    Input: Two bounding boxes
    Output: Boolean indicating overlap
    Unpack coordinates from box1 and box2
    overlap_x = not (xmin1 > xmax2 or xmax1 < xmin2)
    overlap_y = not (ymin1 > ymax2 or ymax1 < ymin2)
    Return overlap_x and overlap_y
end function
function CHECK_FOR_OVERLAPS(shield_coords)
    Input: List of shield coordinates
    Output: Boolean indicating any overlaps
    for each pair of consecutive boxes in shield_coords do
        if boxes overlap according to check_overlap then
            Return True
        end if
    end for
    Return False
end function
function FIND_OVERLAPS(shield_coords)
    Input: List of shield coordinates
    Output: Dictionary of overlapping pairs
    Initialize overlaps as an empty dictionary
    Initialize processed_pairs as an empty set
    for each pair of boxes in shield_coords do
        if boxes overlap according to check_overlap then
            Add overlap to overlaps dictionary
            Add pair to processed_pairs
        end if
    end for
    Return overlaps
end function
```

2.2. Graphical user interface (GUI)

The GUI of the RAPTOR-AI in action is shown in Fig. 1. The developed GUI provides the users with the ability to control their modeling setup through a simple and easy to use interface. In addition, the uploaded image and the image with detected features will be shown in the GUI; this is particularly useful for user to perform preliminary assessments on the precision of the object detection AI module that is built-in the RAPTOR-AI. The domain dimensions which is essentially the width and height of the 2D markup image is also reported; this is particularly important for users to understand the size of their modeled domain and the respective positions of human phantom (shown as black circles) and slab shielding (shown as blue rectangles). We refer the interested readers to the online user manual of RAPTOR-AI at: https://raptorai.io/ for step-by-step tutorial of the developed GUI.

2.3. Human phantom position and slab shielding

The position of human phantom and slab shielding would be defined over the user uploaded image using black dot and rectangles,

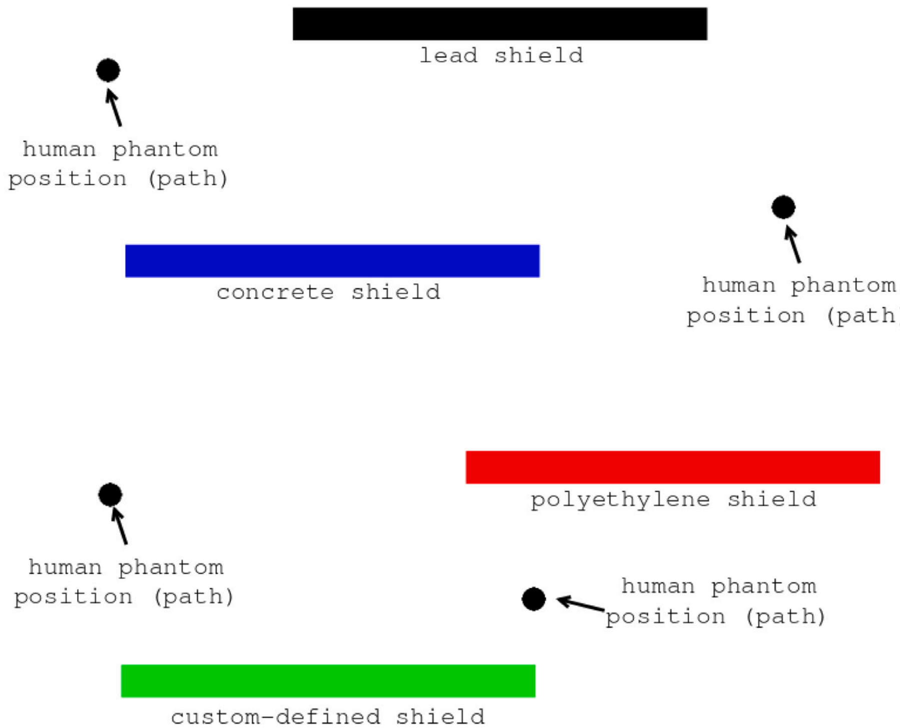

Fig. 2. Schematic diagram showing the positions of human phantom (black circles) and slab shielding materials (rectangles) with different colors.

Algorithm 3 continuation of The Developed Phantom and Model Generator Module Algorithm

function PHANTOM(countx, count, imgw, imgh, x, y, RI, proj, activity, tally, maxcas, maxbch, scale, sx, sy, sz, shieldcount, xmins, xmaxs, ymins, ymaxs, shield_coords)
  Input: Simulation parameters
  Read and parse `config.ini` to extract material properties
  Initialize directories and file paths
  Compute scaling and transformation parameters
  Write simulation parameters, sources, materials, surfaces, and cells to input file
  if `shieldcount` > 0 **then**
    Check for overlaps using `check_for_overlaps`
    Identify overlapping regions with `find_overlaps`
    Write shield materials and their properties
  end if
  Finalize and close files
  if `count` == `countx` **then**
    if `runphits` == 1 **then**
      Execute PHITS simulation
    end if
    if `backup` == 1 **then**
      Create backup of simulation files
    end if
  end if
end function

respectively. In addition, the black, blue, red and green rectangle colors correspond to lead, concrete, polyethylene and custom-defined shielding materials, respectively. Our developed model was trained to detect black circles as human phantom positions over the modeled domain (i.e., image area) and rectangles as slab shields. In addition, the developed model has the ability to detect overlap between the slab shields and resolve them automatically in the final generated PHITS script. The positions of the human phantom and slab shields are shown schematically in Fig. 2.

Our object detection AI model was trained to detect and label these features accordingly. For example, blue color rectangle boxes would be detected and labeled as concrete shielding, while black color rectangles will be detected and labeled as lead shielding. It needs to be noted that multiple shielding materials can be modeled in one model, and the program was developed to automatically resolve overlaps between shielding materials. However, users must note that overlaps between human phantom and the shielding materials are not permitted and therefore must be avoided.

Recent studies have demonstrated significant progress in developing advanced materials for radiation shielding applications through innovative synthesis methods and detailed structural analyses. For instance, several works have focused on thin films, examining the effects of dopants such as boron and rare-earth elements on ZnO, In_2O_3, and other semiconductor matrices (Eskalen et al., 2020; Kavun et al., 2021, 2022; Soğuksu et al., 2024). Others have investigated various glass systems – reinforced by nanoparticles or doped with elements such as Gd_2O_3 and vanadium pentoxide - -to optimize gamma and neutron attenuation, mechanical stability, and thermal resilience (Eskalen et al., 2023; Kavgacı et al., 2024; Kavgacıet al., 2024; Yorulmaz et al., 2024; Kavun et al., 2024). Concurrently, metal alloys (e.g., Al50B25Mg25, CoCrFeNiAg) have been explored, revealing that controlled compositional adjustments and microstructural tuning can enhance both thermal performance and radiation shielding capability (Yaykaşlıet al., 2022a, 2024a, 2022b, 2024b). Further research has expanded to composite concretes and fiber-reinforced systems, highlighting the importance of particle size and fiber choice in achieving robust mechanical properties alongside effective radiation attenuation (Kavun and Eken, 2024). In future versions of RAPTOR-AI we aim to include these advanced materials as shielding in the model.

2.4. Computational scheme

In order to test the present toolkit, we have chosen four different cases with various different human phantom positions, shielding sizes

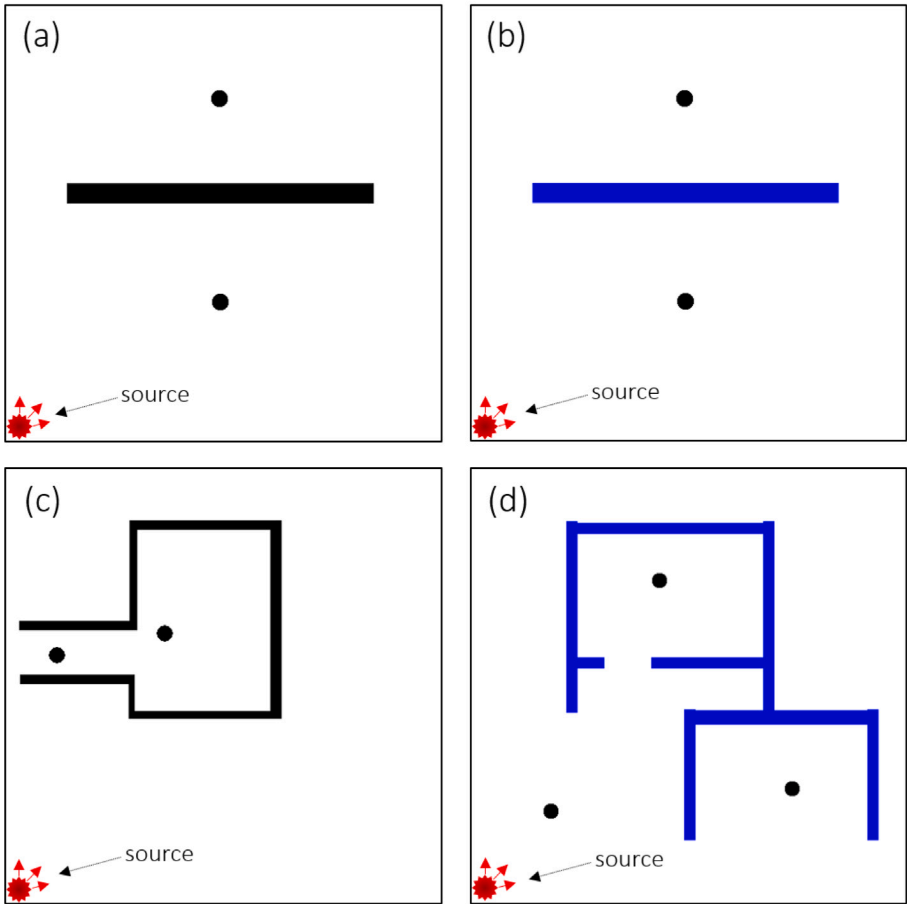

Fig. 3. Cases with different human phantom position and shielding materials considering the present computational scheme.

and materials. These fours cases are shown in Fig. 3 and the position of the source for all cases was kept fixed at (0,0) which corresponds to the bottom left corner of the images. These images were directly fed into the RAPTOR-AI program and the generated PHITS script was then automatically generated for every case.

A total of three main different tallies will be generated for every user-defined case, namely, (1) T-Gshow, (2) T-Deposit that generate 2D geometrical view and dose deposition plots and (3) T-Deposit dose deposition in six selected organs, namely, (1) left lung, (2) right lung, (3) heart tissue and blood, (4) spine and discs, (5) brain and (6) head and face skin. The track length estimate of energy deposition in each organ domain were used by defining the regions into the tally to calculate the dose. In this program, which supports multiple particle types including protons, neutrons, photons, and alpha particles, different physics models are employed to calculate dose deposition, depending on the specific particles and radioisotopes involved. For charged particles, the Intra-Nuclear Cascade Liege (INCL) model was utilized to describe the nuclear reactions relevant to this study. Specifically, the INCL model is the default choice for simulating proton-induced nuclear reactions. The stopping powers for charged particles and nuclei were determined using the ATIMA code https://web-docs.gsi.de/~weick/atima/. For uncharged particles, the Kerma approximation was applied to estimate energy deposition, using the T-Deposit tally function provided by the PHITS MC package. For further details on the physical models employed in the calculation of dose deposition, we refer interested readers to Sato et al. (2018) and the references therein.

The calculation speed of both RAPTOR-AI and the PHITS Monte Carlo package is highly dependent on several factors, including the complexity of the supplied 2D markup images – which directly influences the number of 3 dimensional features – and the available computational resources, such as the number of CPU cores and overall system performance. Additionally, simulation parameters, like the number of particle histories, affect the trade-off between speed and statistical accuracy, with simpler configurations often yielding results in minutes and more complex scenarios extending to hours.

3. Results and discussion

3.1. 3D visualization of the generated models

The 3D visualization of the generated models using the RAPTOR-AI are shown in Fig. 4 (from the top view) that corresponds to the 2D images shown in Fig. 3. Considering these 3D visualizations, it can be seen that the present RAPTOR-AI model has the ability to successfully create the simulation domain based on the supplied markup images; this was generated based on the number of human phantom positions that were marked on the inputs images. In addition, all the MC model parameters supplied by the users were integrated into the generated models.

3.2. 2D dose distribution plots

Considering the generated models, the 2D dose distribution from the top view for the case in Fig. 4(d) is shown in Fig. 5. There are three different human phantom positions in these irradiation scenarios and the dose dispersion can be observed from the top view in the modeled geometry. The human phantom get the highest dose in the case shown in Fig. 5(a), mainly due to its close proximity to the radioactive source (located at 0,0 location) and also absence of any shielding materials. All these 2D dose distribution plots will be automatically generated by the RAPTOR-AI model based on the user-defined cases.

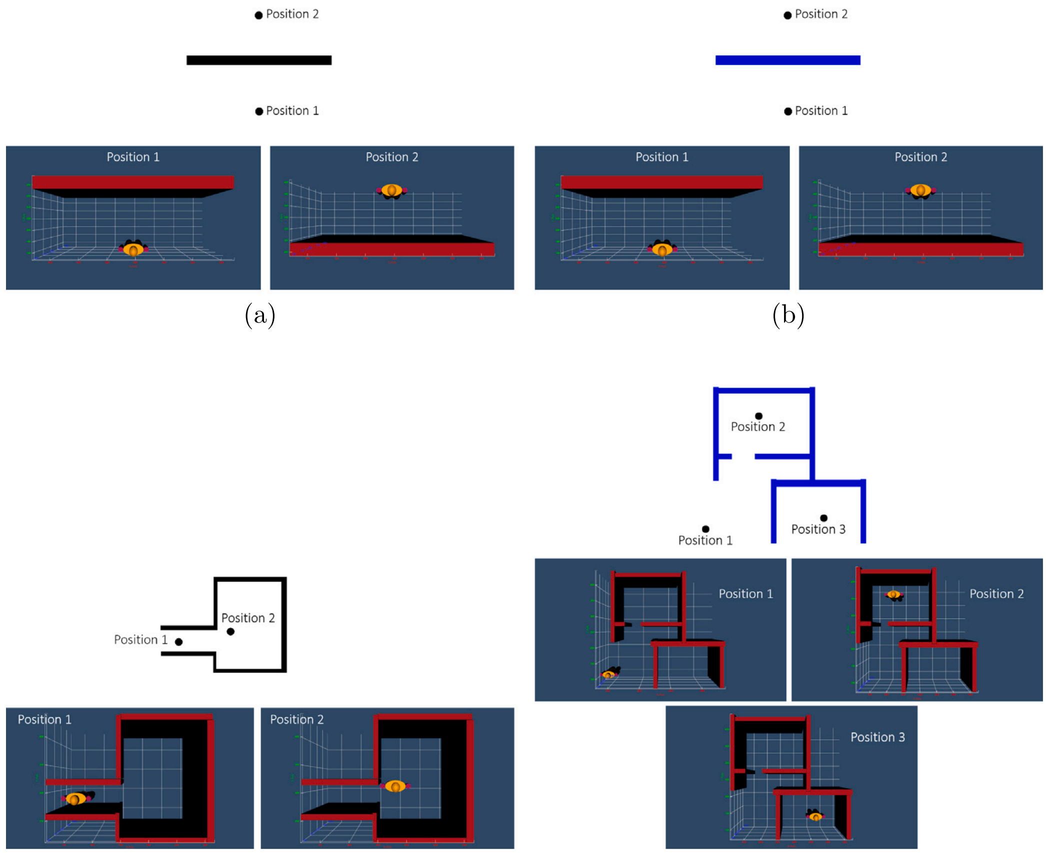

Fig. 4. 3D visualizations from the generated models using RAPTOR-AI from the supplied markup images. The human phantom and generated walls can be seen from the top view.

3.3. Organ doses at different positions and models

A total of six selected organs, namely, (1) left lung, (2), right lung, (3) heat tissue and blood, (4) spine and discs, (5) brain and (6) head and face skin were chosen to score the absorbed doses from 1000 Bq Cs-137 point source. The dose in these organs for cases shown in Fig. 4 were summarized in Fig. 6.

The absorbed doses in different organs generally reduced for positions of human phantoms behind the modeled lead and concrete shielding; this matches well with our previous studies on effect of slab shielding and the dose reduction (Shahmohammadi Beni et al., 2021). In addition, the orientation of the human phantom position with respect to the radioactive point source influences the absorbed dose in different organs.

Considering that the source is located behind the human phantom and to the left side corner of the modeled domain, the highest absorbed dose was found to be in the spine and discs for position with no shielding material. Similarly, the dose in left lung for cases without shielding were found to be higher than the right lung, given that the source is located at the bottom left corner of the modeled domain. The results in Fig. 6 show that RAPTOR-AI model has the ability to successfully simulate human phantom movements in the modeled domain and perform organ specific dosimetry in presence or absence of slab shielding. We refer the readers to our previous works (Watabe et al., 2024b) for details about organ specific dosimetry.

4. Summary and conclusions

In this work, an open-source computational platform named RAPTOR-AI has been developed, capable of performing MC simulations using 2D markup images. These images employ black circles and differently colored rectangles to represent the positions of a human phantom and different shielding materials, respectively. The state-of-the-art, real-time object detection system YOLO (You Only Look Once) version 5 (Redmon et al., 2016), based on Yolov1-Yolov4 (Xu et al., 2021), was utilized to train an AI model for detecting these features. The detected elements were then used to generate a PHITS MC script based on user-defined parameters and the features of the 2D markup images.

Several test cases were conducted to validate the platform, demonstrating that the RAPTOR-AI model is capable of successfully performing MC computations in conjunction with the PHITS package. This tool is expected to be valuable for: (1) robust MC modeling in radiation protection, (2) studying dose dispersion from radioactive materials in emergency situations where time is critical, and (3) quickly conducting radiation protection assessments in emergencies when a structural map of a facility is available, by creating a 2D markup image and using RAPTOR-AI for rapid analysis.

Lastly, RAPTOR-AI is crucial for several reasons: (1) rapid decision making: In emergencies, such as nuclear accidents or radioactive material spills, time is critical. RAPTOR-AI enables quick modeling of radiation environments, allowing first responders and decision-makers to assess radiation risks and implement protective measures rapidly. (2) real-time simulation: The ability to generate MC simulations from simple 2D markup images allows for fast evaluation of shielding effectiveness, reducing the time needed to design or assess protective barriers in the field. (3) accurate dose estimation: RAPTOR-AI can quickly predict dose dispersion in complex environments, helping to prioritize evacuation routes, determine safe zones, and allocate resources efficiently in life-threatening situations. (4) adaptability: In dynamic environments, such as a rapidly evolving radiation leak or an unfamiliar facility, responders can quickly create 2D representations

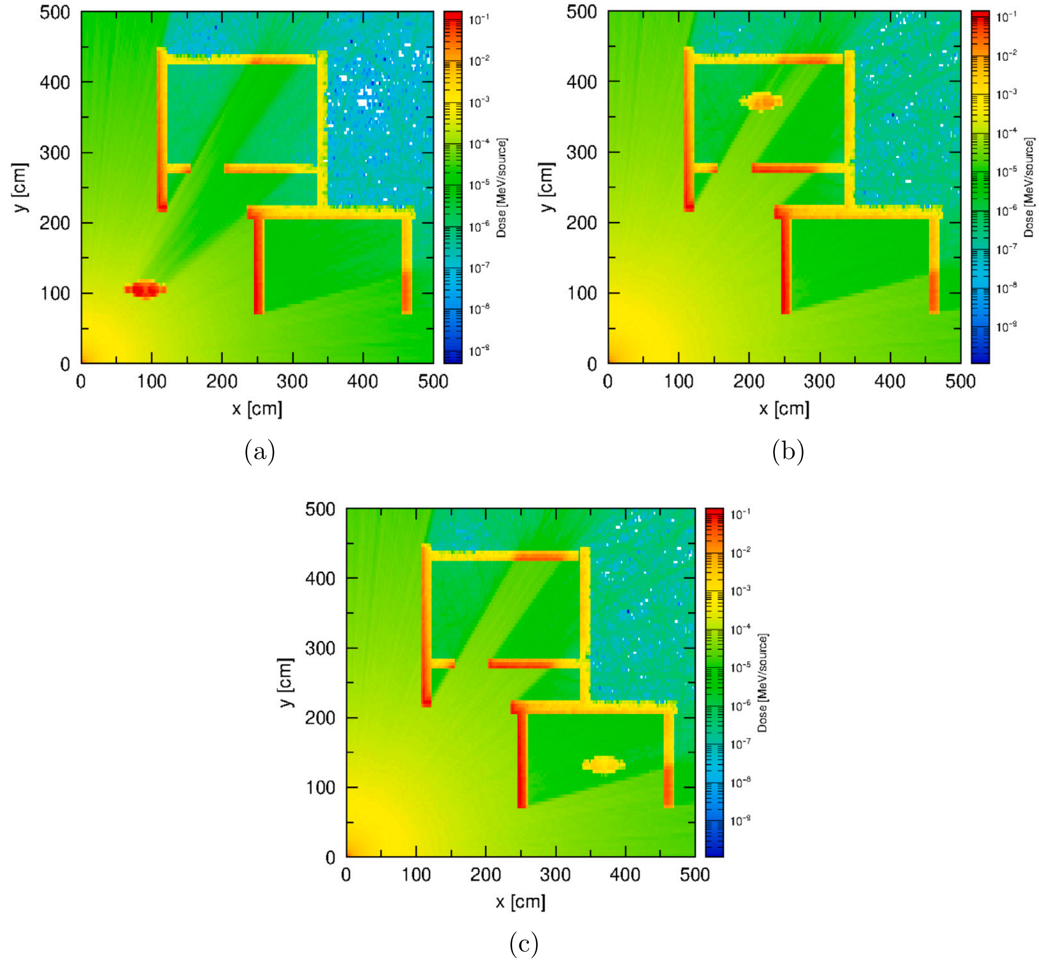

Fig. 5. 2D dose distribution for three different human phantom positions from a 1000 Bq Cs-137 point source.

of the scene and simulate radiation protection measures, improving response times and safety. These capabilities make it highly useful for emergency preparedness, response, and mitigation efforts.

CRediT authorship contribution statement

Hiroshi Watabe: Visualization, Validation, Investigation, Funding acquisition, Formal analysis, Data curation. **Peter K.N. Yu:** Validation, Investigation, Funding acquisition, Data curation. **Dragana Krstic:** Validation, Methodology. **Dragoslav Nikezic:** Visualization, Investigation. **Kyeong Min Kim:** Writing – review & editing, Visualization. **Taiga Yamaya:** Visualization, Investigation. **Naoki Kawachi:** Writing – review & editing, Methodology. **Hiroki Tanaka:** Writing – review & editing, Formal analysis. **Zoran Jovanovic:** Validation, Investigation. **A.K.F. Haque:** Visualization, Validation. **M. Rafiqul Islam:** Visualization, Validation. **Gary Tse:** Writing – review & editing, Validation. **Quinncy Lee:** Writing – review & editing, Validation. **Mehrdad Shahmohammadi Beni:** Writing – review & editing, Writing – original draft, Visualization, Validation, Supervision, Software, Resources, Project administration, Investigation, Formal analysis, Conceptualization.

Declaration of competing interest

The authors declare that they have no known competing financial interests or personal relationships that could have appeared to influence the work reported in this paper.

Acknowledgments

The present work was supported by the JSPS KAKENHI Grant Numbers 21F21103, JPJSBP120218804, 23H03774 and 23K07087, the research Grants 9229151 and 9220124 from City University of Hong Kong. The authors would like to express their sincere gratitude to Prof. Tatsuhiko Sato from Japan Atomic Energy Agency for his invaluable support in this work.

Declaration of competing interest

The authors declare that they have no known competing financial interests or personal relationships that could have appeared to influence the work reported in this paper.

Appendix A. Supplementary data

Supplementary material related to this article can be found online at https://doi.org/10.1016/j.apradiso.2025.111797.

Data availability

All data, executables and source code files and program manual can be downloaded from: https://figshare.com/articles/software/RAPTOR-AI_--_Radiation_Protection_Toolkit_for_Radioisotopes_with_Artificial_Intelligence/26751967and the user-manual can be found from: https://raptorai.io/.

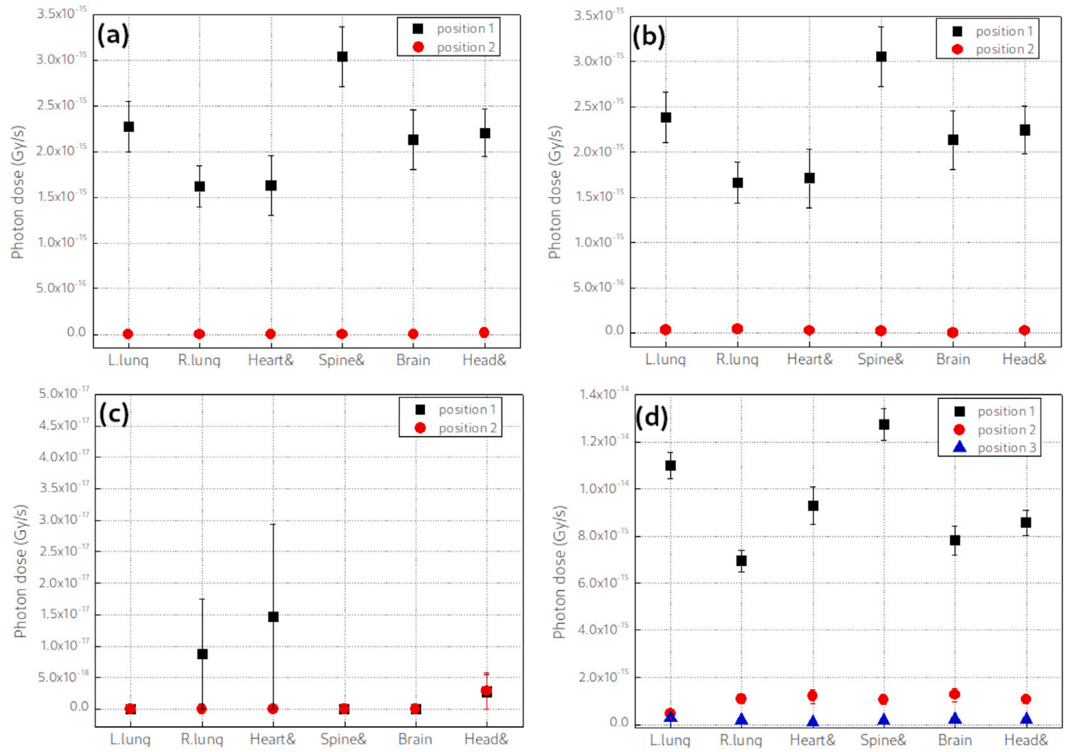

Fig. 6. Dose deposition in six selected organs upon exposure to photons emitted from 1000 Bq Cs-137 radioisotope for four different cases shown in Fig. 3.

References

Acebrón, J.A., Ribeiro, M.A., 2016. A Monte Carlo method for solving the one-dimensional telegraph equations with boundary conditions. J. Comput. Phys. 305, 29–43.

Agostinelli, S., Allison, J., Amako, K.A., Apostolakis, J., Araujo, H., Arce, P., Asai, M., Axen, D., Banerjee, S., Barr, GJ, Behner, F., 2003. GEANT4—a simulation toolkit. Nucl. Instrum. Methods Phys. Res. A 506 (3), 250–303.

Aygün, B., 2021. Neutron and gamma radiation shielding Ni-based new-type superalloys development and production by Monte Carlo simulation technique. Radiat. Phys. Chem. 188, 109630.

Badhwar, G.D., 1997. The radiation environment in low-Earth orbit. Radiat. Res. 148 (Suppl. 5), S3–S10.

Böhlen, T.T., Cerutti, F., Chin, M.P., Fassò, A., Ferrari, A., Ortega, P.G., Mairani, A., Sala, P.R., Smirnov, G., Vlachoudis, V., 2014. The FLUKA code: developments and challenges for high-energy and medical applications. Nucl. Data Sheets 120, 211–214.

Eskalen, H., Kavun, Y., Kavgacı, M., 2023. Preparation and study of radiation shielding features of ZnO nanoparticle reinforced borate glasses. Appl. Radiat. Isot. 198, 110858.

Eskalen, H., Kavun, Y., Kerli, S., Eken, S., 2020. An investigation of radiation shielding properties of boron doped ZnO thin films. Opt. Mater. 105, 109871.

Ferrari, A., Sala, P.R., Fasso, A., Ranft, J., 2005. FLUKA. CERN-library 55 (99), 100, Available at: http://fluka.web.cern.ch/fluka.

Goorley, T., James, M., Booth, T., Brown, F., Bull, J., Cox, L.J., Durkee, J., Elson, J., Fensin, M., Forster, R.A., Hendricks, J., Features of MCNP6. In: SNA+MC 2013—Joint International Conference on Supercomputing in Nuclear Applications Monte Carlo 2014. EDP Sciences, p. 06011.

Goorley, T., et al., 2012. Initial MCNP6 release overview. Nucl. Technol. 180 (3), 298–315.

Hsiao, Y., Stewart, R.D., 2007. Monte Carlo simulation of DNA damage induction by x-rays and selected radioisotopes. Phys. Med. Biol. 53 (1), 233.

Iwase, H., Niita, K., Nakamura, T., 2002. Development of general-purpose particle and heavy ion transport Monte Carlo code. J. Nucl. Sci. Technol. 39 (11), 1142–1151.

Kavgacı, M., Gülpak, H., Eskalen, H., Kavun, Y., Yaykaşlı, H., 2024. Radiation-shielding properties of copper-borate glasses enhanced with MgO nanoparticles: Preparation and investigation. Glas. Phys. Chem. 50 (2), 111–126.

Kavgacı, M., Yaykaşlı, H., Eskalen, H., Kavun, Y., Yaşar, M.M., 2024. $BaTiO_3$–B_2O_3–MgO–Na_2O–CaO glass series: Radiation shielding, thermal, and mechanical properties. Nucl. Instrum. Methods Phys. Res. Sect. B 554, 165462.

Kavun, Y., Eken, M., 2024. Investigation of thermal, acoustic, mechanical, and radiation shielding performance of waste and natural fibers. Appl. Radiat. Isot. 214, 111539.

Kavun, Y., Eskalen, H., Kavgacı, M., Yaykaşlı, H., Bahşi, M., 2024. A novel vanadium pentoxide doped glasses characterization for radiation shielding applications. Appl. Radiat. Isot. 203, 111086.

Kavun, Y., Eskalen, H., Kerli, S., Kavgaci, M., 2021. Fabrication and characterization of GdxFe2O3 (100-x)/PVA (x = 0, 5, 10, 20) composite films for radiation shielding. Appl. Radiat. Isot. 177, 109918.

Kavun, Y., Kerli, S., Eskalen, H., Kavgacı, M., 2022. Characterization and nuclear shielding performance of Sm doped In_2O thin films. Radiat. Phys. Chem. 194, 110014.

Khurana, D., Koli, A., Khatter, K., Singh, S., 2023. Natural language processing: state of the art, current trends and challenges. Multimedia Tools Appl. 82 (3), 3713–3744.

Kimura, A., Nadege, M.T., 2020. Roi editing tool using AI for radiotherapy simulation. In: 2020 IEEE Nuclear Science Symposium and Medical Imaging Conference (NSS/MIC). IEEE, pp. 1–3.

Koyuncu, N., Reyhancan, İA., 2020. Dose evaluation of ^{142}Pr radioisotope by Monte Carlo method in eye brachytherapy. Radiat. Phys. Chem. 177, 109150.

Kuramitsu, Y., Taguchi, T., Nikaido, F., Minami, T., Hihara, T., Suzuki, S., Oda, K., Kuramoto, K., Yasui, T., Abe, Y., Ibano, K., 2024. Optimization of laser-driven quantum beam generation and the applications with artificial intelligence. Physics of Plasmas 31 (5).

Le, H.P., Yan, B., Caflisch, R.E., Cambier, J.L., 2017. Monte Carlo simulation of excitation and ionization collisions with complexity reduction. J. Comput. Phys. 346, 480–496.

Peng, Z., Shan, H., Liu, T., Pei, X., Zhou, J., Wang, G., Xu, X.G., 2019. Deep learning for accelerating Monte Carlo radiation transport simulation in intensity-modulated radiation therapy. arXiv. Available at: arXiv:1910.07735.

Redmon, J., Divvala, S., Girshick, R., Farhadi, A., 2016. You only look once: Unified, real-time object detection. In: Proceedings of the IEEE Conference on Computer Vision and Pattern Recognition. pp. 779–788.

Sarrut, D., Etxebeste, A., Muñoz, E., Krah, N., Létang, J.M., 2021. Artificial intelligence for Monte Carlo simulation in medical physics. Front. Phys. 9, 738112.

Sato, T., Iwamoto, Y., Hashimoto, S., Ogawa, T., Furuta, T., Abe, S.I., Kai, T., Tsai, P.E., Matsuda, N., Iwase, H., Shigyo, N., 2018. Features of particle and heavy ion transport code system (PHITS) version 3.02. J. Nucl. Sci. Technol. 55 (6), 684–690.

Shahmohammadi Beni, M., Krstic, D., Nikezic, D., Yu, K.N., 2021. A comparative study on dispersed doses during photon and proton radiation therapy in pediatric applications. PLoS One 16 (3), e0248300.

Shahmohammadi Beni, M., Ng, C.Y., Krstic, D., Nikezic, D., Yu, K.N., 2017. Conversion coefficients for determination of dispersed photon dose during radiotherapy: Nrurad input code for MCNP. PLoS One 12 (3), e0174836.

Shahmohammadi Beni, M., Watabe, H., Krstic, D., Nikezic, D., Yu, K.N., 2021. MCHP (Monte Carlo + human phantom): platform to facilitate teaching nuclear radiation physics. PLoS One 16 (9), e0257638.

Sihver, L., Mancusi, D., Sato, T., Niita, K., Iwase, H., Iwamoto, Y., Matsuda, N., Nakashima, H., Sakamoto, Y., 2007. Recent developments and benchmarking of the PHITS code. Adv. Space Res. 40 (9), 1320–1331.

Singh, V.P., Ali, A.M., Badiger, N.M., El-Khayatt, A.M., 2013. Monte Carlo simulation of gamma ray shielding parameters of concretes. Nucl. Eng. Des. 265, 1071–1077.

Soğuksu, A.K., Kerli, S., Kavun, Y., Alver, Ü., 2024. Synthesis and characterizations of ce-doped ZnO thin films for radiation shielding. Opt. Mater. 148, 114941.

Su, L., et al., 2014. ARCHERRT – A GPU-based and photon-electron coupled Monte Carlo dose computing engine for radiation therapy: Software development and application to helical tomotherapy. Med. Phys. 41 (7).

Unagar, V., Makwana, R., Barala, S.S., Meena, D., Gupta, S.K., Kavun, Y., Mehta, M., Vashi, V., Singh, R.K., Chauhan, R., Mukherjee, S.K., 2024. Monte Carlo analysis of HDPE using PHITS and MCNP for neutron shielding applications. J. Radioanal. Nucl. Chem. 333 (11), 5457–5464.

Watabe, H., Sato, T., Yu, K.N., Zivkovic, M., Krstic, D., Nikezic, D., Kim, K.M., Yamaya, T., Kawachi, N., Tanaka, H., Haque, A.K., 2024b. Development of DynamicMC for PHITS Monte Carlo package. Radiat. Prot. Dosim. 200 (2), 130–142.

Watabe, H., Yu, K.N., Safakatti, N., Beni, M.S., 2023. Development of an open-source GUI computer program for modelling irradiation of multi-segmented phantoms using grid-based system for PHITS. Nucl. Eng. Technol. 55 (1), 373–737.

Watabe, H., Yu, P.K.N., Tse, G., Krstic, D., Nikezic, D., Islam, M.R., Wei, Z., Wei, Y., Beni, M.S., 2024a. Monte Carlo modelling of cyclotron and radioisotope center (CYRIC) at Tohoku university: a radiation protection study. J. Radiol. Prot. 44 (2), 021521.

Xu, R., Lin, H., Lu, K., Cao, L., Liu, Y., 2021. A forest fire detection system based on ensemble learning. For. 12, 217.

Yaykaşlı, H., Eskalen, H., Kavun, Y., Gögebakan, M., 2022a. Microstructural, thermal, and radiation shielding properties of $Al_{50}B_{25}Mg_{25}$ alloy prepared by mechanical alloying. J. Mater. Sci.: Mater. Electron. 33 (5), 2350–2359.

Yaykaşlı, H., Eskalen, H., Kavun, Y., Gögebakan, M., Kaya, A.H., 2024a. Microstructure and thermal and radiation shielding properties of CoCrFeNiAg high entropy alloy. J. Mater. Eng. Perform. 33 (18), 9686–9698.

Yaykaşlı, H., Eskalen, H., Kavun, Y., Gögebakan, M., Kaya, A.H., 2024b. Microstructure and thermal and radiation shielding properties of CoCrFeNiAg high entropy alloy. J. Mater. Eng. Perform. 33 (18), 9686–9698.

Yaykaşlı, H., Eskalen, H., Kavun, Y., M., Gögebakan, 2022b. Microstructural, thermal, and radiation shielding properties of $Al_{50}B_{25}Mg_{25}$ alloy prepared by mechanical alloying. J. Mater. Sci.: Mater. Electron. 33 (5), 2350–2359.

Yorulmaz, N., Yasar, M.M., Acikgoz, A., Kavun, Y., Demircan, G., Kamislioglu, M., Aktas, B., Ulas, E.O., 2024. Influence of Gd_2O_3 on structural, optical, radiation shielding, and mechanical properties of borate glasses. Opt. Mater. 149, 115032.

Yu, K.N., Watabe, H., Zivkovic, M., Krstic, D., Nikezic, D., Kim, K.M., Yamaya, T., Kawachi, N., Tanaka, H., Haque, A.K., Beni, M.S., 2023. DynamicMC: an open-source GUI program coupled with MCNP for modeling relative dynamic movement of radioactive source and ORNL phantom in a 3-dimensional radiation field. Heal. Phys. 124 (4), 301–309.

Zhao, Z.Q., Zheng, P., Xu, S.T., Wu, X., 2019. Object detection with deep learning: a review. IEEE Trans. Neural Netw. Learn. Syst. 30 (11), 3212–3232.

Zou, Z., Chen, K., Shi, Z., Guo, Y., Ye, J., 2023. Object detection in 20 years: A survey. Proc. IEEE 111 (3), 257–276.